

Figure 1.9 Heat storage project (schematic) at the Science City Campus (Hönggerberg) of ETH Zurich (Switzerland). (Courtesy of ETH Zurich, Abteilung Bau, 2011.)

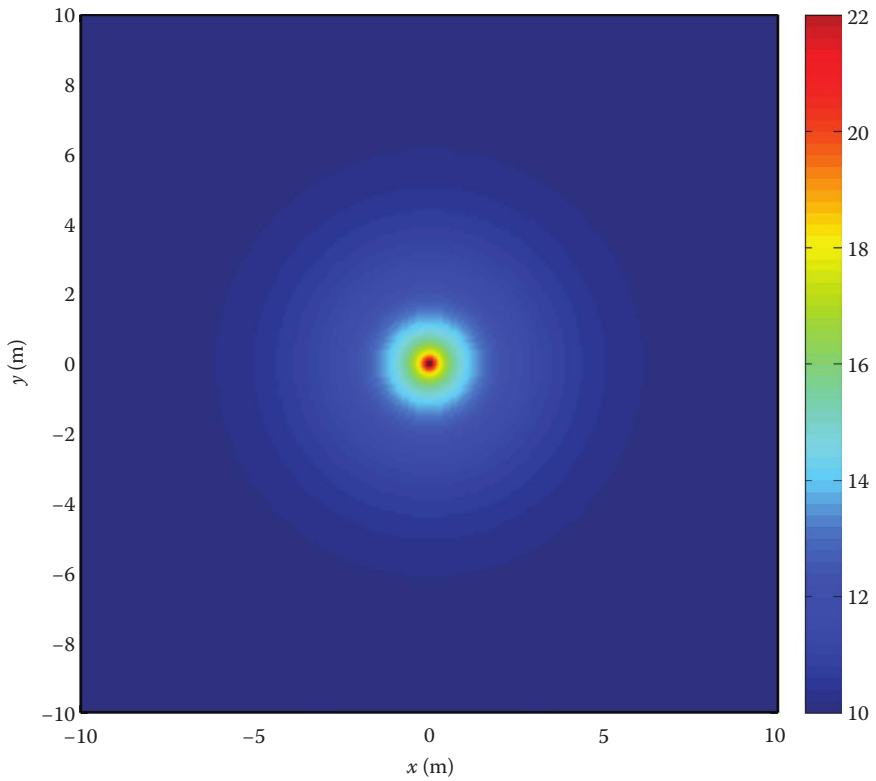


Figure 3.2 Temperature field for a single BHE with constant energy extraction after 90 days. ILS model ($q_{tb} = J/H = 50 \text{ W m}^{-1}$, $T_0 = 10^\circ\text{C}$, $D_t = 9 \times 10^{-7} \text{ m}^2 \text{ s}^{-1}$).

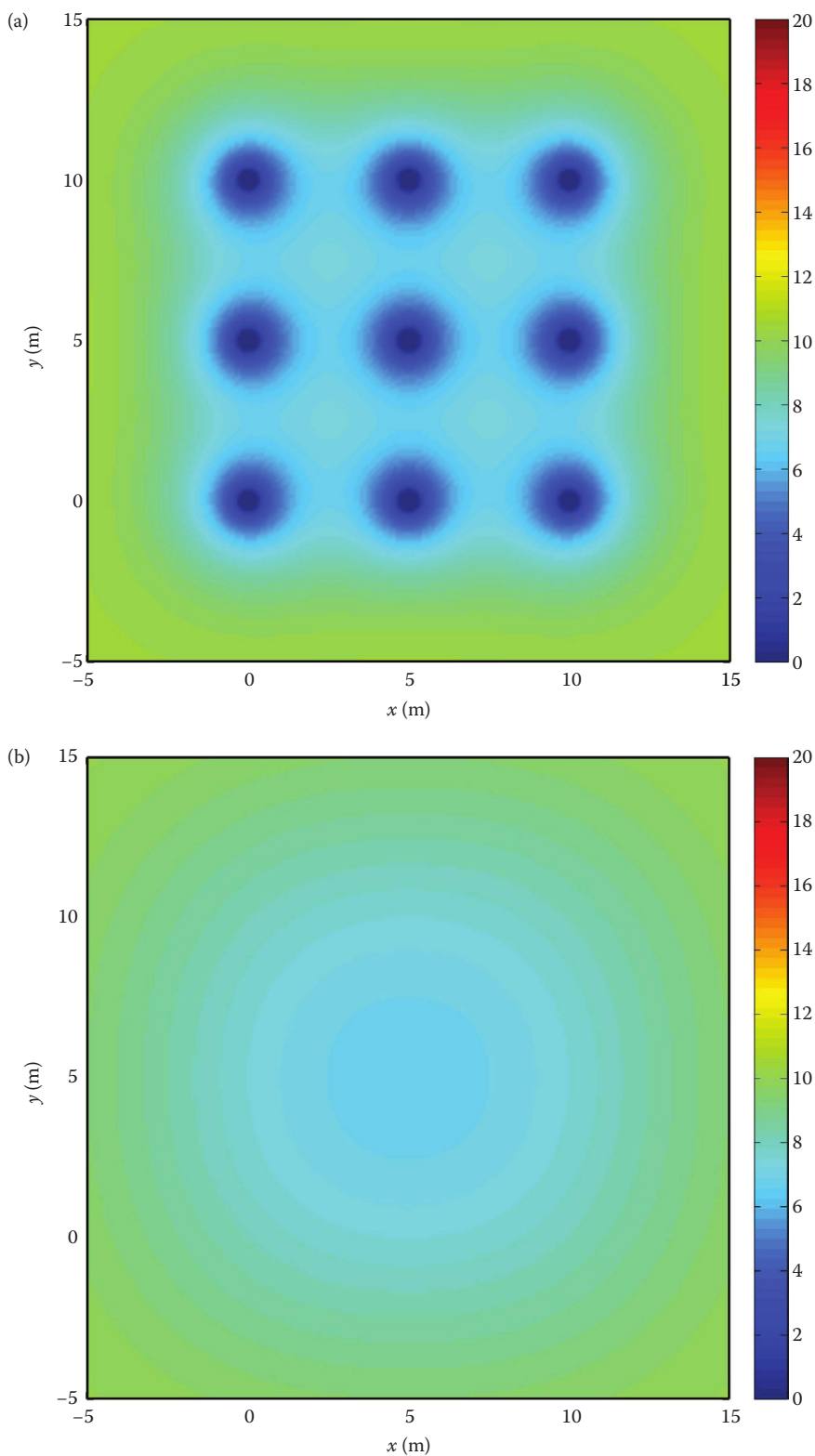


Figure 3.4 Heat exchanger group 3×3 calculated with ILS model with seasonal cosine heat input. (a) Map after 10.0 years; (b) 10.25 years; (c) 10.5 years; and (d) 10.75 years.

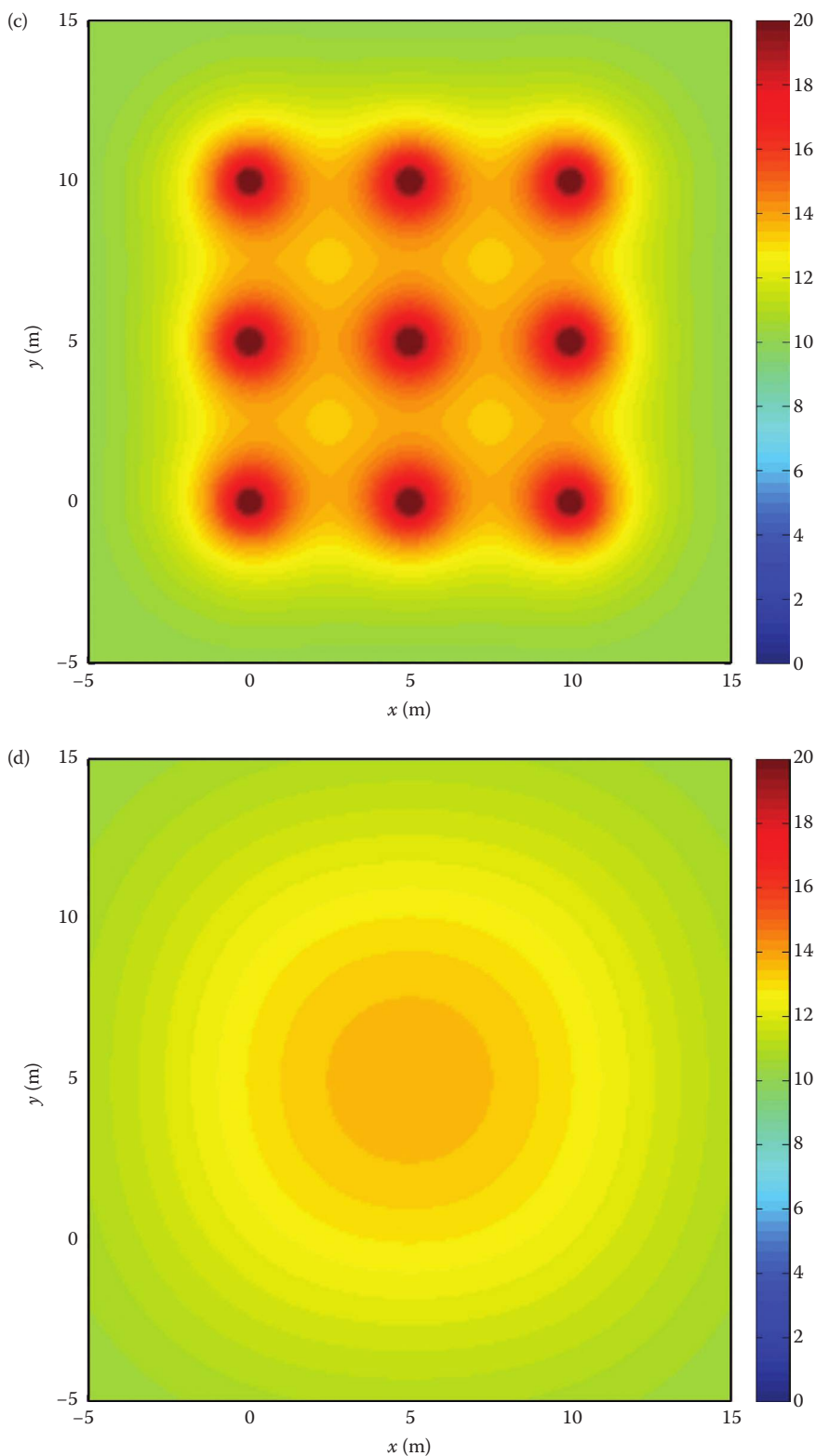


Figure 3.4 (Continued) Heat exchanger group 3×3 calculated with ILS model with seasonal cosine heat input. (a) Map after 10.0 years; (b) 10.25 years; (c) 10.5 years; and (d) 10.75 years.

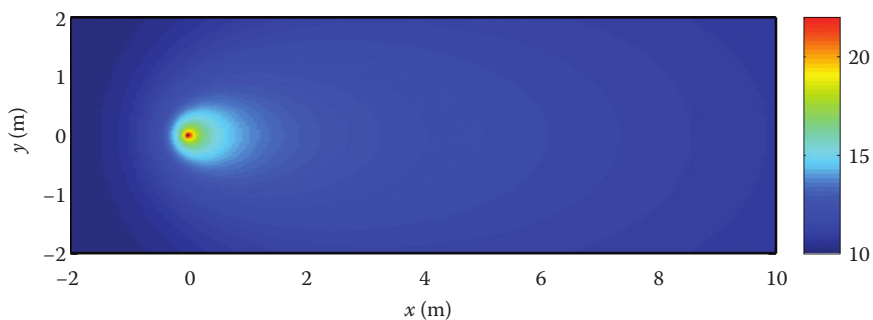


Figure 3.12 Temperature field for a single BHE with constant energy extraction after 90 days ($q_{tb} = J/H = 50 \text{ W m}^{-1}$, $T_0 = 10^\circ\text{C}$, $q = 1.0 \times 10^{-6} \text{ m s}^{-1}$, $D_t = 9 \times 10^{-7} \text{ m}^2 \text{ s}^{-1}$).

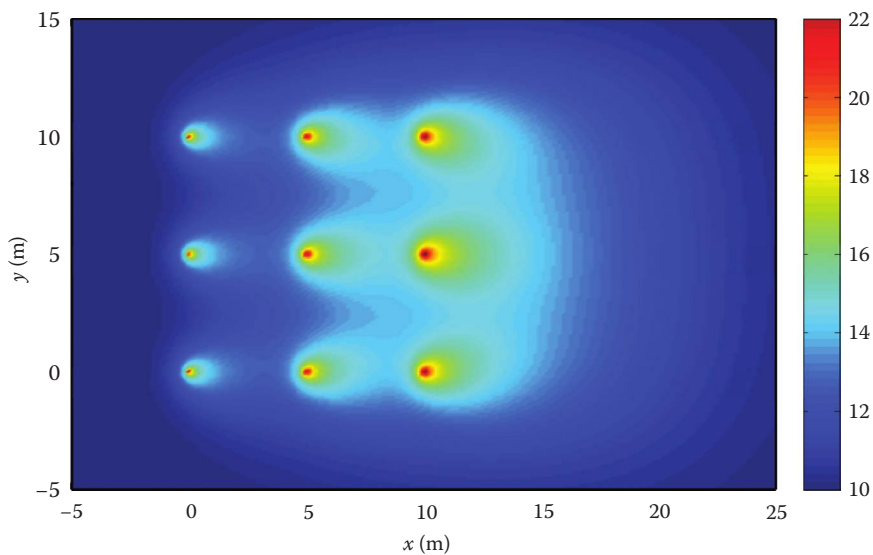


Figure 3.13 Temperature field of multiple interacting BHEs with constant energy extraction after 90 days ($q_{tb} = J/H = 50 \text{ W m}^{-1}$, $T_0 = 10^\circ\text{C}$, $q = 1.0 \times 10^{-6} \text{ m s}^{-1}$, $D_t = 9 \times 10^{-7} \text{ m}^2 \text{ s}^{-1}$).

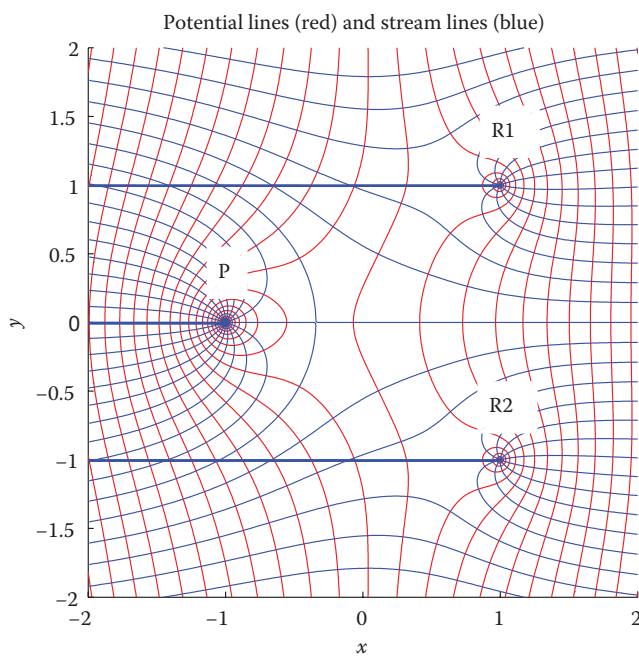


Figure 3.24 Scaled flow field with $\alpha = 0$ and scaled pumping rate; one pumping well and two injection wells. P: pumping well; R1, R2: recharge wells.

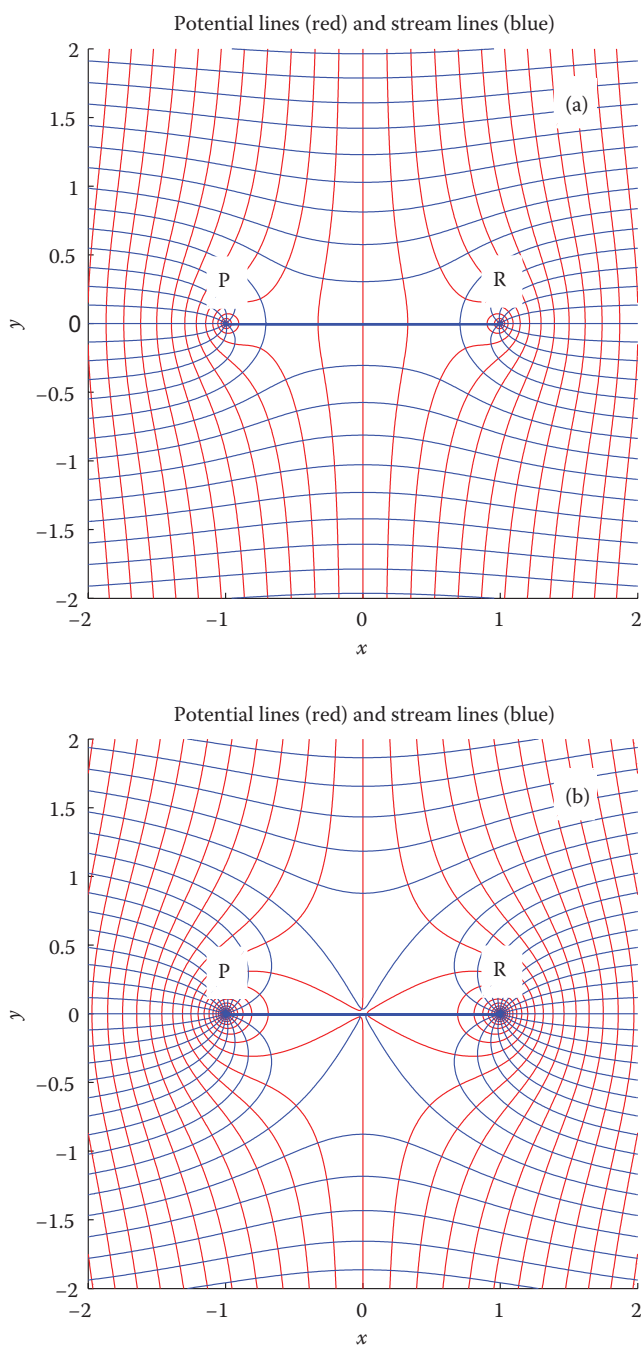


Figure 3.25 (a) Scaled flow field with $\alpha = 0$ and scaled pumping rate $\chi = 0.5$. P: pumping well; R: recharge well. (b) Scaled flow field with $\alpha = 0$ and $\chi = 1$. (c) Scaled flow field with $\alpha = 0$ and $\chi = 2$. (d) Scaled flow field with $\alpha = 90^\circ$ and $\chi = 1$.

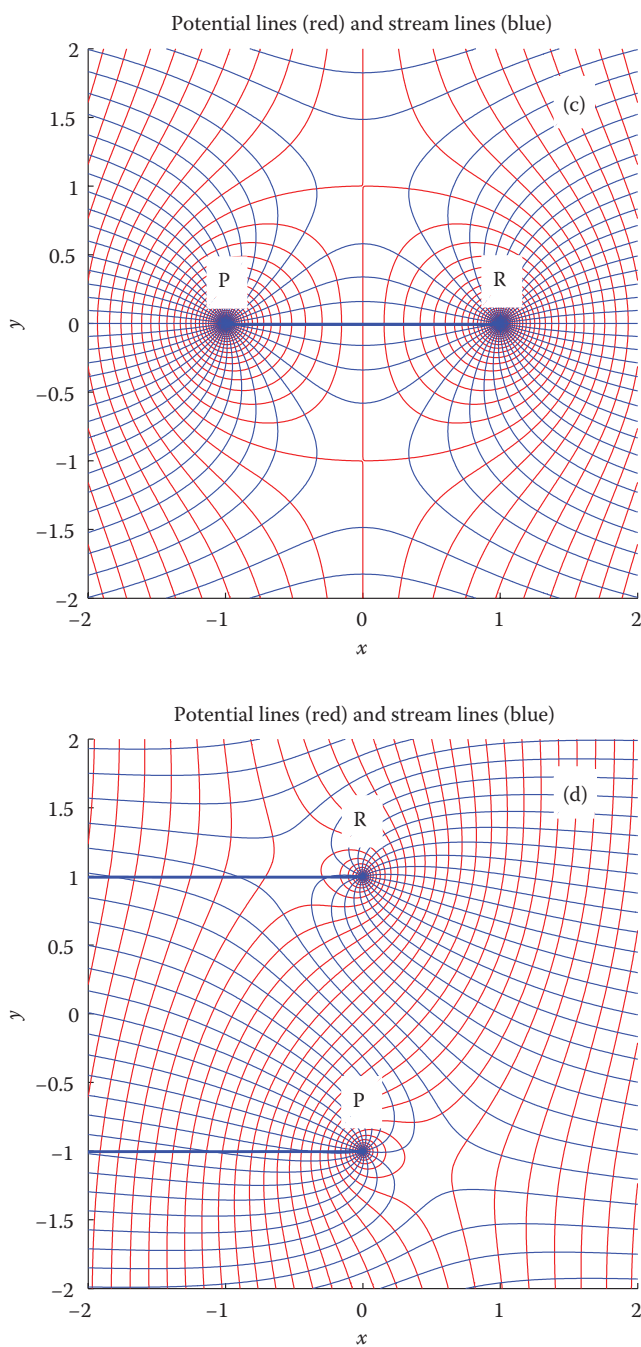


Figure 3.25 (Continued) (a) Scaled flow field with $\alpha = 0$ and scaled pumping rate $\chi = 0.5$. P: pumping well; R: recharge well. (b) Scaled flow field with $\alpha = 0$ and $\chi = 1$. (c) Scaled flow field with $\alpha = 0$ and $\chi = 2$. (d) Scaled flow field with $\alpha = 90^\circ$ and $\chi = 1$.

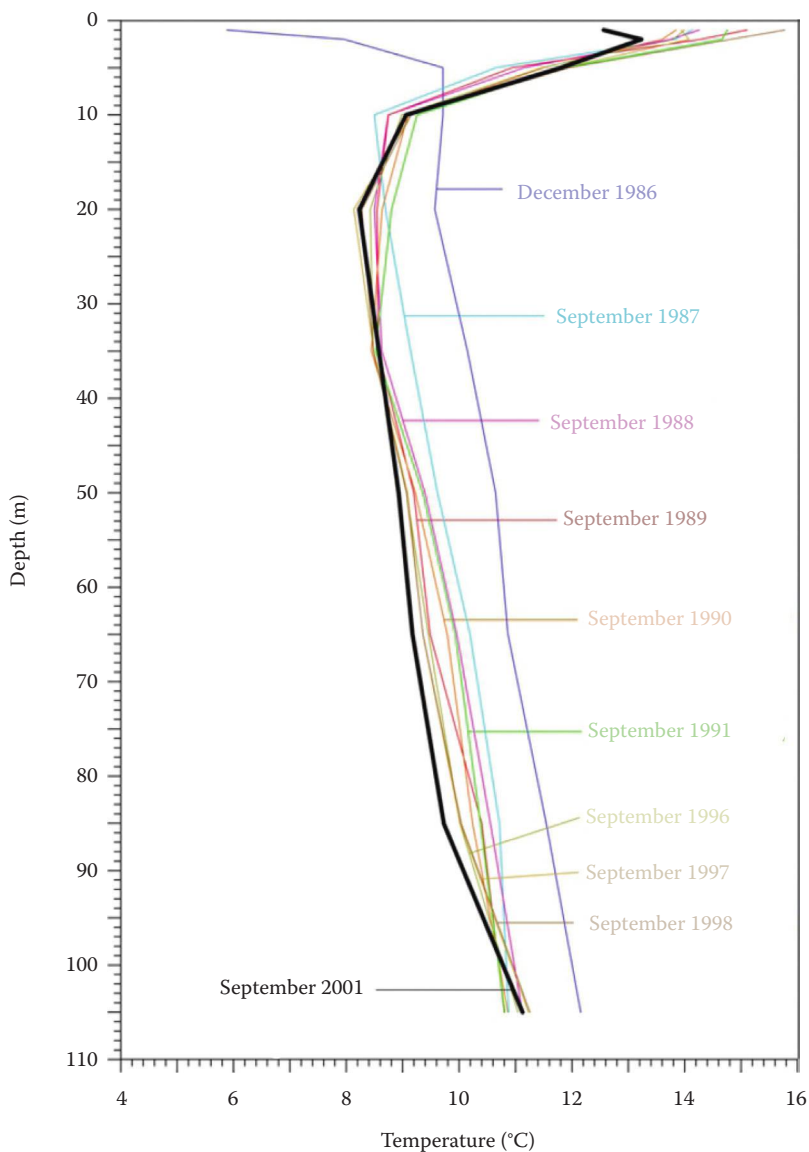


Figure 5.2 Elgg site (Switzerland): measured ground temperature profiles at 0.5 m distance from a 105 m deep operating BHE, repeatedly measured over 15 years. (From Rybach, L. and Eugster, W.J., *Geothermics* 39, 365–369, 2010.)

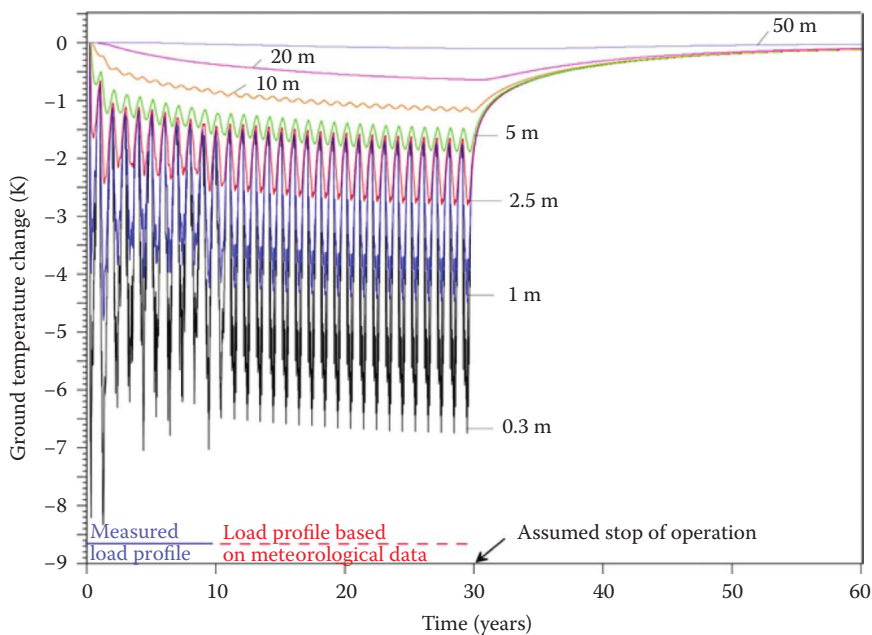


Figure 5.3 Elgg site (Switzerland): simulated ground temperature changes of a BHE relative to the undisturbed situation in December 1986 over 30 years of operation and 30 years of recovery. (From Rybach, L. and Eugster, W.J., *Geothermics* 39, 365–369, 2010.)

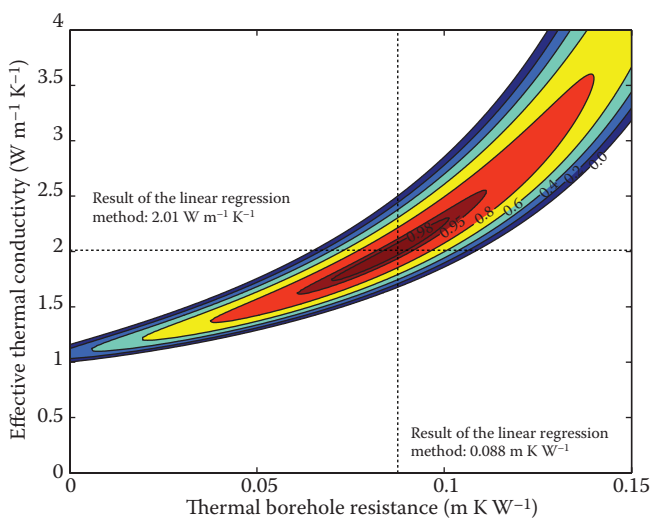


Figure 6.5 Example of the parameter estimation technique for the evaluation of the thermal borehole resistance and the effective thermal conductivities showing the results of the model efficiencies (EF values) according to Loague and Green (1991). The results of the linear regression method are also shown. (From Wagner 2010.)

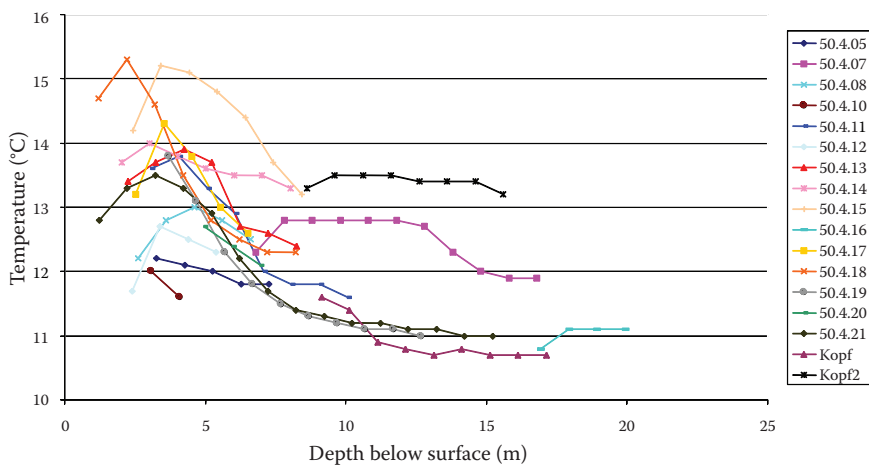


Figure 7.1 Altach study: temperature profiles in boreholes, measured on November 13, 2001. (Modified after Cathomen, N., Wärmetransport im Grundwasser, Auswirkungen von Wärmepumpen auf die Grundwassertemperatur am Beispiel der Gemeinde Altach im Vorarlberger Rheintal. Diploma thesis, ETH Zurich, Institute of Hydromechanics and Water Resources Management, 2002.)

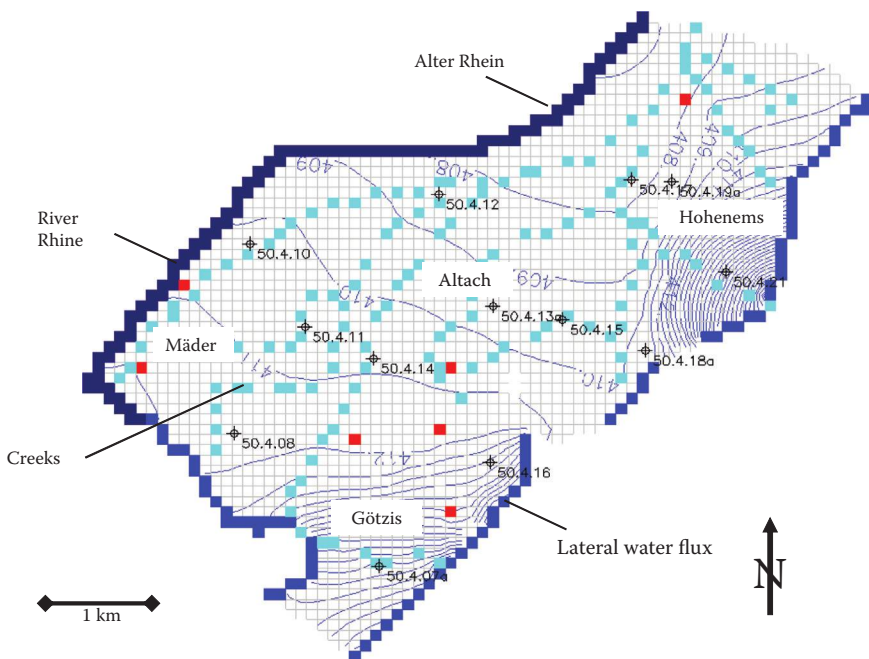


Figure 7.2 Altach study: two-dimensional flow model Altach (Austria) with head isolines (equidistance 1 m). Dark blue: river cells; blue: prescribed inflow cells; bright blue: creeks. (Modified after Cathomen, N., Wärmetransport im Grundwasser, Auswirkungen von Wärmepumpen auf die Grundwassertemperatur am Beispiel der Gemeinde Altach im Vorarlberger Rheintal. Diploma thesis, ETH Zurich, Institute of Hydromechanics and Water Resources Management, 2002.)

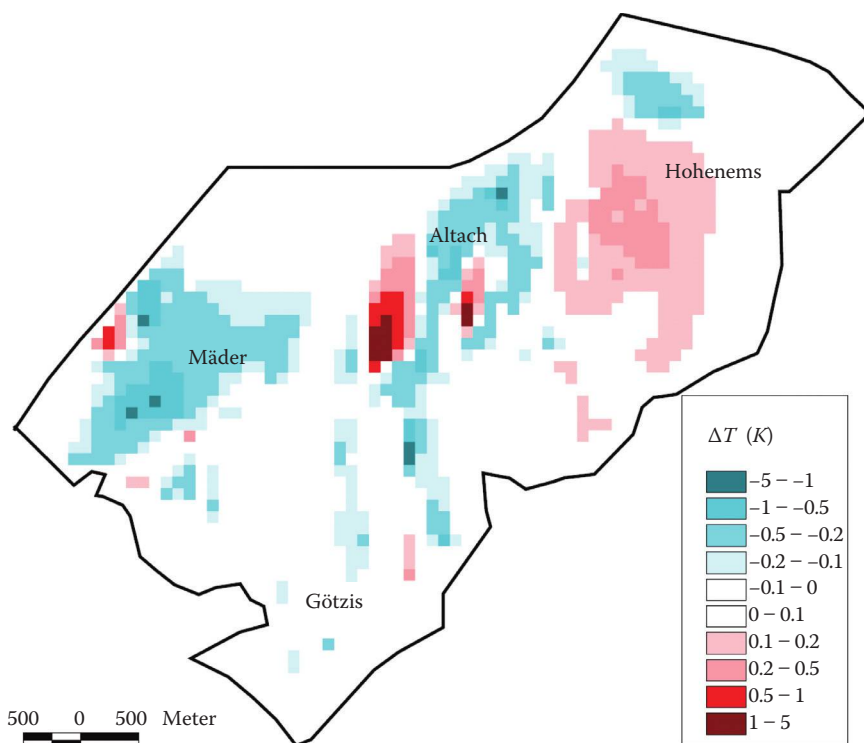


Figure 7.3 Altach study: two-dimensional heat transport model Altach (Austria) with temperature increase due to thermal use (groundwater heat pumps, heating by constructions). Dark blue: river cells; blue: prescribed inflow cells. (Modified after Cathomen, N., Wärmetransport im Grundwasser, Auswirkungen von Wärmepumpen auf die Grundwassertemperatur am Beispiel der Gemeinde Altach im Vorarlberger Rheintal. Diploma thesis, ETH Zurich, Institute of Hydromechanics and Water Resources Management, 2002.)

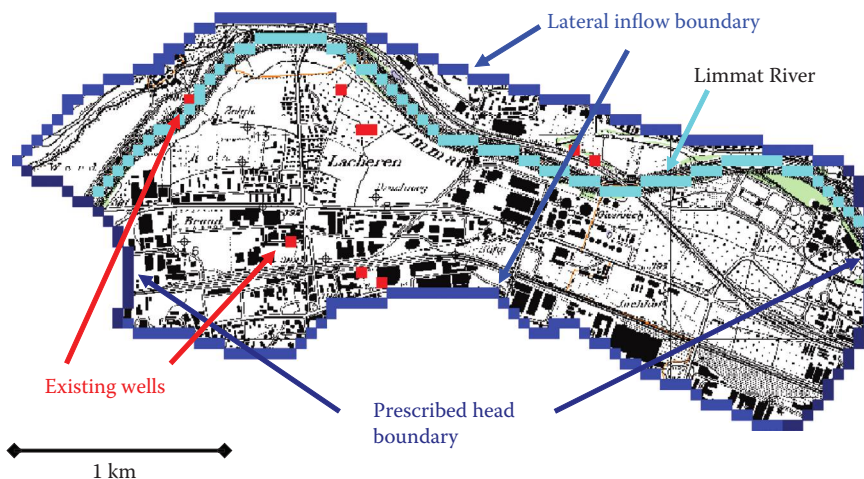


Figure 7.4 Case study Limmat Valley, subregion town of Schlieren: model domain with wells, and boundary conditions. (Modified after Müller, E., Ott, D., Thermische Nutzung des Grundwasserleiters Limmattal, Teilgebiet Hardhof-Schlieren [Thermal use of the Limmat Valley aquifer: Area Hardhof-Dietikon]. Report Master Project, ETH Zurich, Institute of Environmental Engineering, 2005.)

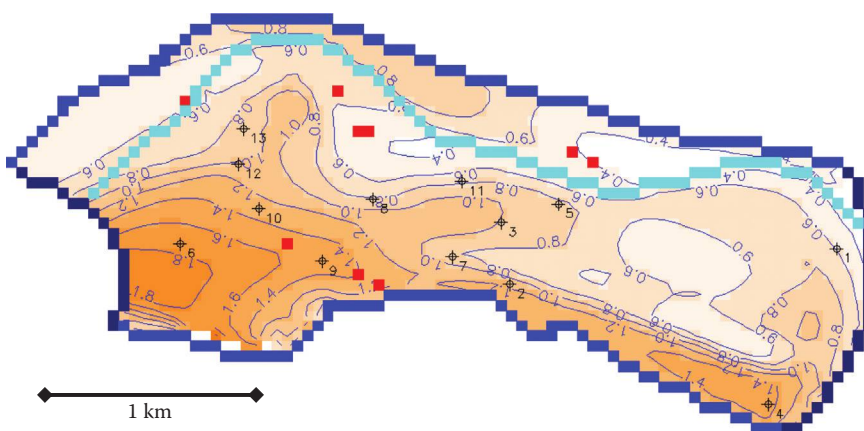
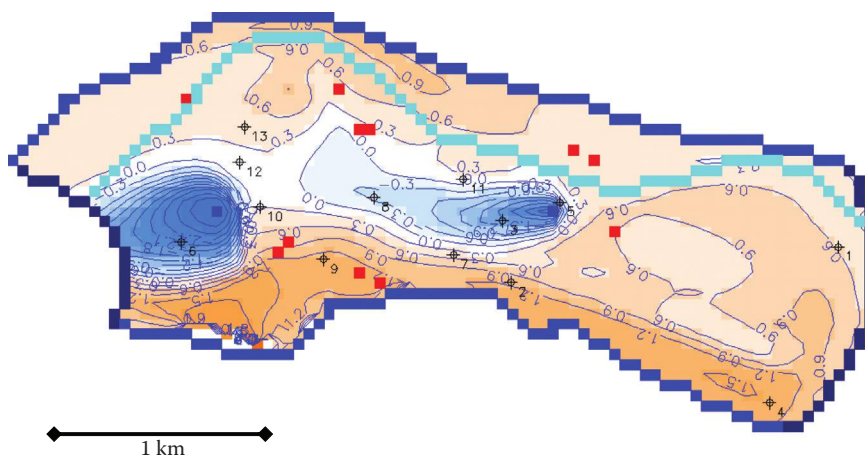


Figure 7.5 Case study Limmat Valley, subregion town of Schlieren: quasi-steady-state simulation of the temperature increase by warm basements. (Modified after Müller, E., Ott, D., Thermische Nutzung des Grundwasserleiters Limmattal, Teilgebiet Hardhof-Schlieren [Thermal use of the Limmat Valley aquifer: Area Hardhof-Dietikon]. Report Master Project, ETH Zurich, Institute of Environmental Engineering, 2005.)



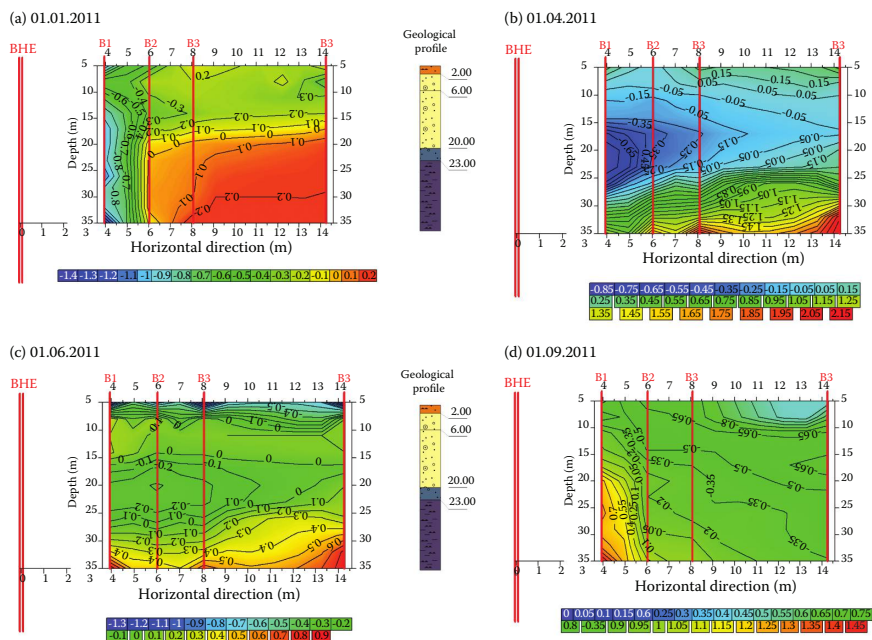


Figure 7.9 Bad Wurzach study: cross section of the temperature measurements in various depths in groundwater flow direction over a time period of one year.

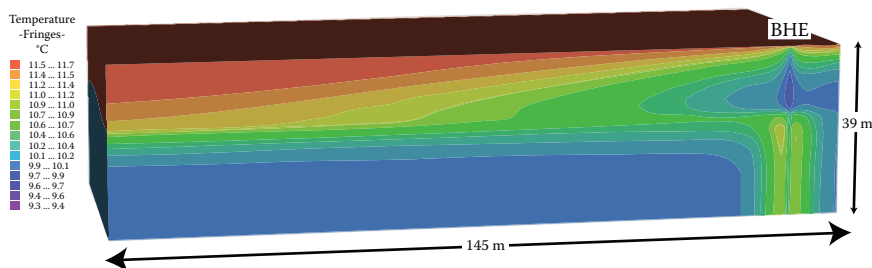


Figure 7.10 Bad Wurzach study: 3D numerical heat transport model of the BHE (EWI/09) showing the resulting temperature plume after 160.4 days.

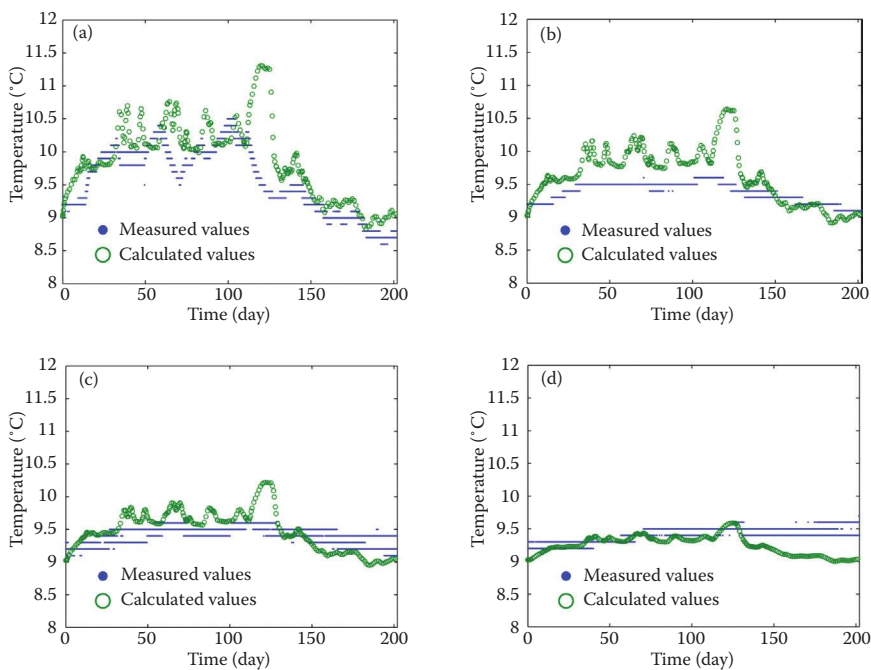


Figure 7.11 Bad Wurzach study: comparison between measured and simulated temperatures at the four observation wells (a) B1, (b) B2, (c) B3, and (d) B4 in 21 m depth in the vicinity of the BHE (EW1/09).